Available online at www.sciencedirect.com

ScienceDirect

www.elsevier.com/locate/jes

JES JOURNAL OF ENVIRONMENTAL SCIENCES

www.jesc.ac.cn

Effects of benthic hydraulics on sediment oxygen demand in a canyon-shaped deep drinking water reservoir: Experimental and modeling study

Nan Li[1,2], *Tinglin Huang*[1,2,*], *Zhiying Chang*[1,2], *Kai Li*[1,2]

[1] *Key Laboratory of Northwest Water Resource, Environment and Ecology, MOE, Xi'an University of Architecture and Technology, Xi'an 710055, China*

[2] *Shaanxi Key Laboratory of Environmental Engineering, Xi'an University of Architecture and Technology, Xi'an 710055, China.*

ARTICLE INFO

Article history:
Received 2 July 2020
Revised 21 September 2020
Accepted 21 September 2020
Available online 8 October 2020

Keywords:
Sediment oxygen demand
Sediment-water flux
Diffusive boundary layer thickness
Turbulence
Biological oxygen consumption

ABSTRACT

Sediment oxygen demand (SOD) is a major contributor to hypolimnetic oxygen depletion and the release of internal nutrient loading. By measuring the SOD in experimental chambers using in both dissolved oxygen (DO) depletion and diffusional oxygen transfer methods, a model of SOD for a sediment bed with water current-induced turbulence was presented. An experimental study was also performed using near-sediment vertical DO profiles and correlated hydraulic parameters stimulated using a computational fluid dynamics model to determine how turbulences and DO concentrations in the overlying water affects SOD and diffusive boundary layer thickness. The dependence of the oxygen transfer coefficient and diffusive boundary layer on hydraulic parameters was quantified, and the SOD was expressed as a function of the shear velocity and the bulk DO concentrations. Theoretical predictions were validated using microelectrode measurements in a series of laboratory experiments. This study found that flow over the sediment surface caused an increase in SOD, attributed to enhanced sediment oxygen uptake and reduced substances fluxes, i.e., for a constant maximum biological oxygen consumption rate, an increased current over the sediment could increase the SOD by 4.5 times compared to stagnant water. These results highlight the importance of considering current-induced SOD increases when designing and implementing aeration/artificial mixing strategies.

Introduction

Oxygen depletion in stratified lakes and reservoirs can have deleterious impacts on water quality and aquatic ecosystems (Beutel et al., 2014; Dutton et al., 2018). During stratification periods, the hypolimnion is isolated from sources of reaeration (e.g., the atmosphere and phytoplankton photosynthesis) and dissolved oxygen (DO) is quickly consumed by the mineralization of organic matter and respiration of microorganisms in the water column or within the upper sediments (Schwefel et al., 2018; Zhang et al., 2021). If the oxygen demand exceeds the total oxygen mass of the bottom water, anoxia occurs initially at the sediment-water interface and then extends upwards into the water layers (Li et al., 2019). Hypolimnetic anoxia can lead to the release of soluble chemical species

* Corresponding author.
E-mail: huangtinglin@xauat.edu.cn (T. Huang).

https://doi.org/10.1016/j.jes.2020.09.020
1001-0742/

(e.g., phosphorus, nitrogen, methylmercury, hydrogen sulfide, iron, and manganese) from the sediments (Beutel et al., 2014; Matzinger et al. 2010; Ito and Momii, 2015). Quantitatively determining the amount of oxygen demand due to the decomposition of organic matter and microorganism activity in the water column and sediment-water interface (SWI) is crucial for optimizing water quality and managing lakes and reservoirs (Bryant et al., 2011a).

Oxygen demand in the hypolimnion is comprised of water oxygen demand and sediment oxygen demand (SOD) by the diagenesis of particulate organic matter, biological respiration and oxidation of reduced compounds diffusing upward from the sediment (Beutel et al., 2007; Yan et al., 2020). SOD is a primary sink for DO in the hypolimnion and is particularly sensitive to near-sediment hydrodynamics, DO concentrations, and intrinsic sediment characteristics (Bierlein et al., 2017; Schwefel et al., 2017). The bottom boundary layer (BBL) adjacent to the sediment is a major energy sink for basin-scale currents due to bottom friction and breaking of propagating internal waves on sloping bottoms (Lorke et al., 2003). Wüest et al. (2000) have shown that 90% of the energy that enters the stratified lakes dissipates through friction within the BBL, while Jabbari et al. (2020) reported that turbulence in the BBL significantly influences the mass transport to the sediments. Approaching the sediment, a thin diffusive boundary layer (DBL), with a few millimeters of thickness (δ_{DBL}), regulates the O_2 flux across the SWI via molecular diffusion (Jørgensen and Revsbech, 1985). As a result, turbulence in the BBL controls the thickness of the DBL and, subsequently, the flux of O_2 into the sediment. Elevated currents velocity of the bottom water tends to decrease δ_{DBL} at the sediment-water interface, thereby increasing the SOD (Bryant et al., 2010b).

The SOD is typically determined by DO depletion in bulk water within a closed chamber (SOD_b) (Beutel, 2003) or by sediment oxygen uptakes (J_{O_2}) at the SWI via microelectrode sensors (Arega and Lee, 2005). Studies have found that water velocity and DO concentrations over the sediment have a dramatic effect on SOD, even when sediment resuspension is not observed (Beutel et al., 2007; Bowman and Delfino 1980). While several studies have found that turbulence can markedly increase the SOD in a chamber, the quantitative relationship between SOD and the turbulence intensity remains unclear (Beutel, 2003). With the help of high-resolution measurements of oxygen profiles at the SWI using microelectrodes, the effect of turbulences on oxygen distribution at the SWI and the corresponding J_{O_2} have been observed (Bryant et al., 2010b; Schwefel et al., 2018). New insights have been gained from theoretical studies regarding how turbulence variation impacts the J_{O_2} in laboratory experiments (Higashino et al., 2008). Meanwhile, in situ experiments have confirmed the theoretical prediction of seiche-induced turbulences on the J_{O_2}, δ_{DBL}, and sediment oxic zone depth (Bryant et al., 2010a).

In deep lakes and reservoirs, the benthic water column is relatively stable and the near-bottom current velocity is usually in the range of a few mm/sec to approximately 10 cm/sec (Wüest and Lorke, 2003). The techniques employed to solve the hypolimnion anoxia (e.g., hypolimnetic oxygenation systems, artificial destratification systems, and water-lifting aerators) can largely increase the water currents and the DO concentrations over the sediment, thereby markedly increasing the SOD compared to that of stagnant water (Bryant et al., 2011a). Despite theoretical and experimental advances (Beutel, 2003; Wüest and Lorke, 2003) and few in situ experiments performed to resolve the effects of turbulence on SOD (Bryant et al., 2011a; Schwefel et al., 2017), the experimental methods are relatively limited in application. Although isolated measurements have evaluated the SOD via different methods (e.g., SOD_b and J_{O_2}), no single method has proven to be optimal; thus, further comparisons and integrations between the various methods are required (Arega and Lee, 2005; Beutel, 2003).

The objective of this study is to build a SOD model that integrates the different methods (e.g., DO depletion in closed chambers and J_{O_2}) under different mixing levels. We performed an experimental analysis using near-sediment vertical DO profiles and correlated hydraulic parameters stimulated using computational fluid dynamics (CFD) calculations. Then, we determined how turbulences and DO concentrations in the overlying water impact SOD and diffusional oxygen transfer at the SWI in a cylindrical chamber. The results of this study characterize how sediment O_2 dynamics are affected by turbulences over sediment and assess the increases in SOD when hypolimnetic aeration systems are operated in a study reservoir.

1. Materials and methods

1.1. Study site and sediment cores collection

The sediment cores used in the experimental chambers were collected from Jinpen Reservoir (JPR), a typical monomictic drinking water reservoir located in a monsoon climate region, in a heavily forested watershed within the Qinling Mountains (Li et al., 2019). The JPR was built by intercepting a valley in the mountains that has a very steep bottom slope; the average and maximum depths were 70 m and 94 m, respectively. Strong thermal stratification and hypolimnetic anoxia were observed in the reservoir from April to January. To prevent the degradation of water quality near the sediment, the water lifting and aeration systems (WLAs), which combined the functions of hypolimnetic aeration and destratification, was used in the reservoir (Li et al., 2019).

The sediment cores and overlying water were collected at the deepest location in JPR using a gravity sediment core sampler and transported to the laboratory. The overlying water was siphoned from the top and the surface sediment cores (thickness of 7 cm) were cut and slowly placed into a cylindrical plexiglass chamber (Fig. 1). A horizontal angled inflow jet was set at 3 cm above the sediment to create steady three-dimensional swirling laminar flows of different levels. After sediment-water interface samples were collected, a cap with inflow/outflow jets and a gasket were connected with the chamber using glass cement. Then, the chamber was slowly filled with the overlying water for incubation.

1.2. Sediment oxygen demand incubations

Before the experiment, the SOD chambers were incubated in the dark at a constant temperature (7 °C; *in situ* temperature

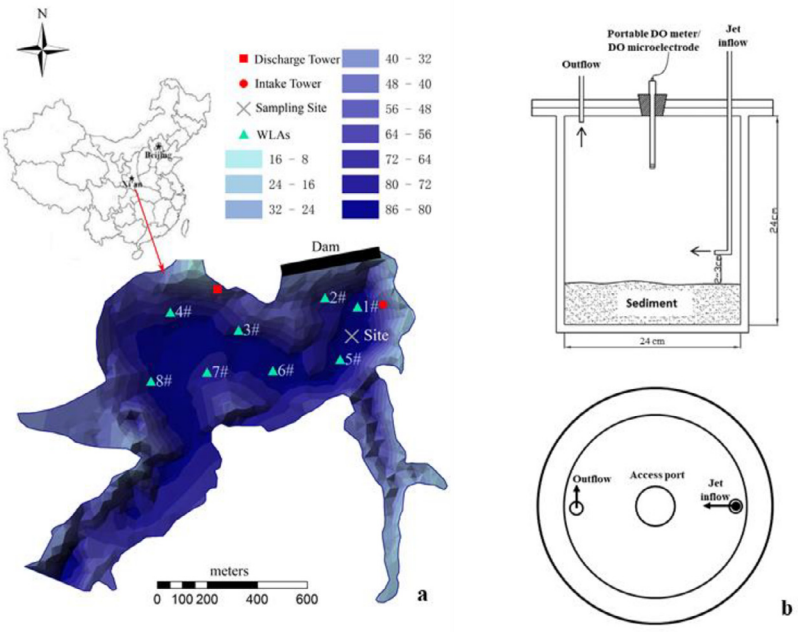

Fig. 1 – Sampling site and a sketch of the experimental sediment oxygen demand (SOD) chambers. (a) Map of Jinpen Reservoir (JPR) showing depth, water-lifting aerators, and locations of sampling sites. The contour plots were drawn based on water depth (m) when the elevation of the water level is 586 m. (b) The SOD chambers were made up of cylindrical plexiglass chambers with inflow/outflow jets on the cap, and had a diameter of 24 cm, and a height of 24 cm.

near sediment) for two days to allow the suspended particles to settle into the sediment. The water columns in the SOD chambers were then gently aerated to saturation, and the visible bubbles were removed from under the cap of the SOD chamber and in the pipe of the peristaltic pump. The chambers were sealed using a rubber plug with a portable DO meter at the access port, and the top of the probe was approximately 2–3 cm above the sediment (Fig. 1). Prior to the measurements, the bulk water in the chambers was well-oxygenated and the DO concentrations in the overlying water were recorded using the probe after a stable reading. The water column was slightly stirred slightly by the water flows circulations, and the velocity of the inflows in jet (u_{in}) was controlled by a peristaltic pump operated at speeds of approximately 0–14 cm/sec. After the chambers were sealed, the DO concentrations were measured continuously (at 2-hr interval) during the study of five to six days until the rate of DO decrease was relatively low. The water oxygen demands were also determined simultaneously in chambers without sediment to determine the oxygen demand exerted only by the sediment.

Identical SOD chambers and operating conditions were used in the measurements of J_{O_2} via microelectrode sensors (Unisense, Denmark). During measurement periods, the SOD chambers were moved out of the incubators and covered in ice to maintain the temperature. Before the measurements, the water in the chambers was aerated to saturation, and then the peristaltic pump was operated at a constant inflow velocity for two hours by regulating the revolutions per minute (r/min). The microprofiles of DO concentrations at the SWI were measured using a Clark-type microelectrode with rapid response time (90 % response in < 8 sec) and a negligible stirring sensitivity inserted through an access port at the top of the chamber. To maintain a steady DO concentration in the overlying water, J_{O_2} was measured under saturation conditions. Measurements were made at 100 μm intervals and the oxygen microsensors were calibrated with anoxic sediment cores and air-saturated overlying water (zero and saturation levels).

1.3. *Calculation of sediment oxygen demand*

1.3.1. *DO depletion in SOD chambers*

The SOD in the closed chambers was evaluated to determine DO whether concentration decreases were zero or first-order versus time (Beutel, 2003):

$$SOD_b = (k_0 - k_w) \times \frac{V}{A} \quad (1)$$

or

$$SOD_b = \frac{(k_1 \times C - k_w) \times V}{A} \quad (2)$$

where k_0 (mg/L/day) and k_1 (mg/L/day) are the sediment-water oxygen consumption rates in zero- and first-order relationships, respectively; k_w (mg/L/day) is the water oxygen consumption rate (in this study, the water oxygen concentrations linearly decrease in chambers without sediment; therefore, k_w is a constant); V (L) is the volume of water in the chambers; and A (m^2) is the area of the sediment-water interface. When the DO concentration linearly decreased over time (zero-order relationship) during SOD measurements, k_0 was calculated

as the slope of the line of best-fit, and the SOD was unrelated to the DO concentrations in the overlying water (Eq. (1)). When the DO concentrations decreased exponentially with time (first-order relationship), the DO oxygen consumption rate k_1 (day^{-1}) was calculated as the slope of the line of best-fit of the natural log of the DO concentration over time. SOD was then calculated as the product of the constant k_1 and the DO concentration in the overlying water minus the water oxygen demand (k_w). To account for the influences of water volume on oxygen demand (e.g., during field studies), both sediment and water oxygen demand were converted to a flux ($g/m^2/day$) by multiplying with the volume of the chamber water and dividing by the sediment-water interface area (Eq. (2)). SOD estimation was classified as linear unless the r^2 value of the exponential model was 0.02 units larger than the r^2 value of the linear model (Beutel et al., 2007).

1.3.2. *Sediment oxygen uptake (J_{O_2})*

J_{O_2} and δ_{DBL} were evaluated based on oxygen distribution at the SWI using Fick's law (Bryant et al., 2011a).

$$SOD_d = J_{O_2} = D\frac{C_{bulk} - C_{SWI}}{\delta_{DBL}} \quad (3)$$

where J_{O_2} ($mg/m^2/day$) is the oxygen flux across the SWI; δ_{DBL} (mm)is the thickness of the diffusive boundary layer in the overlying water directly observed by the O_2 profiles at the SWI; D (m^2/sec) is the diffusion coefficient for oxygen in the overlying water; C_{bulk} (mg/L) is the DO concentration in the overlying water; and the C_{SWI} (mg/L) is the DO concentration at the SWI. The D value was 1.47×10^{-9} m^2/sec at 7 °C.

1.4. *Prediction of δ_{DBL} and SOD under steady flows*

The conceptual framework adopted for the prediction of SOD and δ_{DBL} under steady three-dimensional laminar flows in a cylindrical chamber follows that of Beutel (2003) and Arega and Lee (2005). A near bottom inflow was horizontally set through the glass square bend jets above the sediment. The horizontal velocity of the flow at the center of the chamber linearly increased from zero at the surface sediment to u_0 at the edge of the exterior of the laminar boundary layer (viscous sublayer). The oxygen concentrations in the diffusive boundary layer within the viscous sublayer were therefore linearly distributed; hence, J_{O_2} can be calculated using Fick's law (Beutel et al., 2007) and δ_{DBL} was estimated as (Arega and Lee, 2005):

$$\delta_{DBL} = c_1\frac{\upsilon}{u_*}\,Sc^{-\frac{1}{3}} \quad (4)$$

where c_1 is the numerical constant; υ is the viscosity of the water (1.43×10^{-6} m^2/sec at 7 °C); u_* (m/sec) is the shear velocity; $u_* = \sqrt{\tau_0/\rho}$, where τ_0 (N/m^2) is the bed shear stress; and Sc is the Schmidt number, $Sc = \upsilon/D = 973$ at 7 °C.

The oxygen transfer coefficient K_c in the laminar sublayer was calculated as the ratio of the diffusion coefficient to the δ_{DBL}, and is related to u_* and Sc of the solute as:

$$K_c = \frac{SOD}{C_{bulk} - C_{SWI}} = \frac{D}{\delta_{DBL}} = c_2 u_* Sc^{-\frac{2}{3}} \quad (5)$$

In the present study, $K_c = SOD/(C_{bulk} - C_{SWI})$, from microelectrode measurements. For closed chamber values, the SOD_b includes the oxygen transfer and the reduced flux across the SWI; K_c (as a total oxygen transfer coefficient) was calculated as in Eq. (2). To integrate the two methods, the total K_c was used as a function of $u_* Sc^{-\frac{2}{3}}$.

According to Eqs. (3) and (4), the SOD can be further expressed as:

$$SOD = a_1\frac{D}{\upsilon}\,Sc^{\frac{1}{3}}\,u_*(C_{bulk} - C_{SWI}) = f_* u_*(C_{bulk} - C_{SWI}) \quad (6)$$

where c_2, a_1, and a_2 are numerical constants, $f_* = a_1\frac{D}{\upsilon}\,Sc^{\frac{1}{3}} = a_2 Sc^{-\frac{2}{3}}$, and $f_* u_*$ is expressed as the equivalent of the mass transfer coefficient. According to Fick's law, the J_{O_2} can be estimated from both sides of the SWI (Bryant et al. 2010b). In the diffusive sediment layer, the volumetric rate of oxygen consumption R_s, (defined as D_s (d^2C/d^2y)) is largely controlled by the sediment characteristics and is usually assumed to be constant, and the SOD can be estimated as (Bouldin 1968):

$$SOD = \sqrt{2D_s C_{SWI} R_s} = \sqrt{2D_s C_{SWI}\left(\mu\frac{C_{SWI}}{K_{O_2} + C_{SWI}} + k_1 C_{SWI}\right)} \quad (7)$$

where the D_s (m^2/sec) is the diffusion coefficient for oxygen in sediment; R_s ($g/m^3/day$) is the volumetric rate of oxygen consumption in sediment; μ ($g/m^3/day$) is the maximum biological volumetric sediment oxygen consumption rate; K_{O_2} (g/m^3) is half-saturation constant for DO in Monod expression; and k_1 (day^{-1}) is the first-order rate coefficient. The R_s was made up of the biological and chemical components of the sediment oxygen consumption rate (Arega and Lee, 2005). For certain sediment, the coefficients μ, K_{O_2}, D_s, and Sc are constant, C_{SWI} can be eliminated from the equations, and the SOD depends only on the velocity and DO of the overlying water. Under well-oxygenated conditions, chemical oxidation is negligible and the SOD can be expressed as (Arega and Lee, 2005):

$$\frac{SOD}{\sqrt{2(\mu D_s)C_{bulk}}} = \frac{\sqrt{1+U^2} - 1}{U} \quad (8)$$

and

$$U = u_*\sqrt{\frac{2f_*^2 C_{bulk}}{\mu D_s}} \quad (9)$$

where U is the dimensionless velocity and μD_s is defined as the sediment bioactivity which is constant for a certain sediment. If the friction coefficient f_* is independently measured, then the SOD can be predicted as a function of u_* and C_{bulk} for given sediment. Consequently, the SOD can be expressed as:

$$U = a\frac{\sqrt{1 + (bu_*)^2} - 1}{bu_*} \quad (10)$$

where $a = \sqrt{2(\mu D_s)C_{bulk}}$, and $b = \sqrt{2f_*^2 C_{bulk}/\mu D_s}$, and the constant numbers a and b can be obtained from the best fit curves.

1.5. *Chamber hydraulics*

The cylindrical chamber was initially designed to evaluate the influences of mixing levels on the SOD via DO depletion

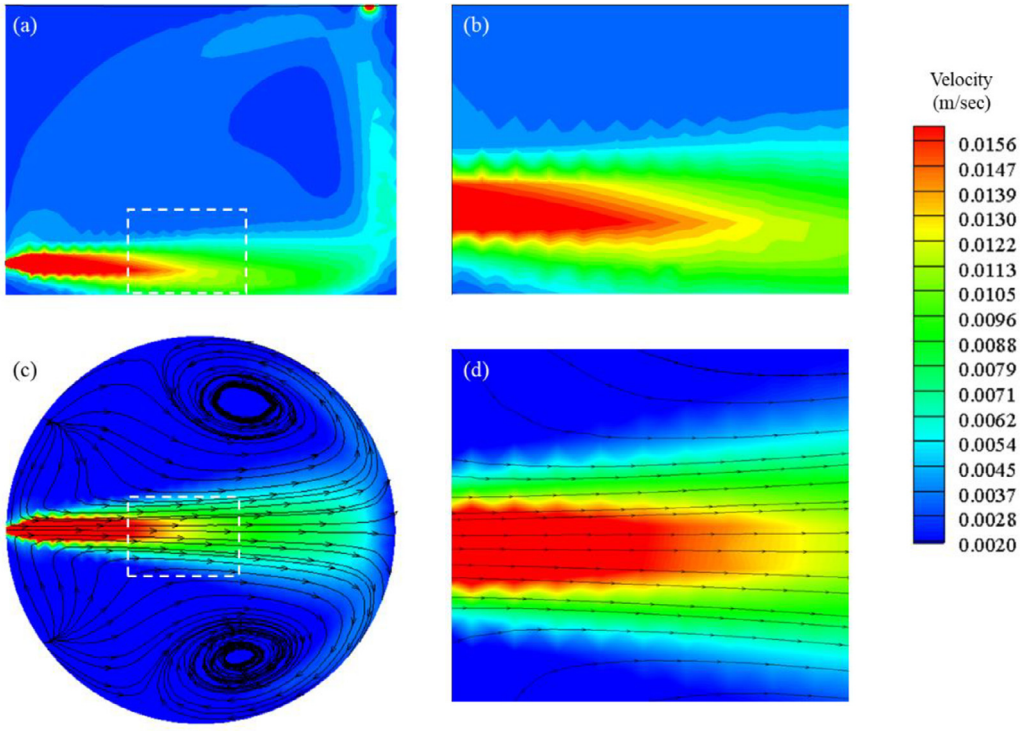

Fig. 2 – (a) Vertical and (c) horizontal distribution of current flows over the sediment (e.g., u_0 = 0.14 cm/sec). Detailed drawings (inside the dashed white squares) of fluid flows along the central axis in vertical and horizontal layers are shown in (b) and (d), respectively.

(Beutel, 2003). The hydraulics of the cylindrical SOD chamber was further modeled in this study to estimate the effects of turbulences in BBL on oxygen transfer at the SWI under well-oxygenated conditions. Steady three-dimensional swirling laminar flows with different levels were computed using the finite volume method. The governing equations during the modeling process included the mass, momentum, energy conservation equations, and the k–ε turbulence model.

The CFD models reveal a highly complicated flow (Fig. 2), characterized by a primarily tangential and near-uniform flow along the central axis in the horizontal layers and a strong swirl induced by the jet inflows. The bulk water was mixed well and a steady laminar layer was obtained over the sediment. The horizontal currents velocity (u_0) at the upper edge of velocity and the corresponding bed shear stress (τ_0) over the sediment in the center of the SOD chamber were stimulated by the CFD models under different inflow velocities (u_{in}) at the jet nozzle. The dissipation of turbulent kinetic energy (ε) and u_*, which were used to characterize the turbulence were calculated as (Bryant et al., 2010a):

$$\varepsilon = \frac{u_*^3}{\kappa h} \tag{11}$$

where k (the von Karman constant) is 0.41 and h is the height above the sediment.

2. Results

2.1. *Sediment oxygen demand determinations*

The determination of SOD using DO depletion and microelectrode measurements is shown in Fig. 3. Substantial variations in the DO concentrations in closed SOD chambers were observed in response to the u_{in} (Fig. 3a). At the beginning of the measurement, the DO concentrations in bulk water were relatively steady with an average value of 9 mg/L. The concentrations, then, decreased exponentially with time by first-order in nature. The corresponding magnitude of the areal rate constant (k, m/day) were 0.024, 0.053, 0.076, and 0.105 m/day, when values of u_{in} were 0, 3, 9, and 15 cm/sec, respectively.

The summary of DO profiles obtained by microelectrode in response to different inflow velocities at the SWI at 7 °C is shown in Fig. 3b. Although the DO concentrations in the overlying water were relatively high (Fig. 3a), the DO concentrations were lower immediately adjacent to the sediment (Fig. 3b). Under quiescent conditions, the DO concentrations above the sediment and at the SWI were 6.9 and 4.7 mg/L, respectively (Fig. 3b), while under mixed conditions, the DO concentrations immediately above the sediment were relatively constant at 8.5 mg/L, and increased from 5.8 to 7.4 mg/L at SWI in response to higher inflow velocities. Turbulences near the sediment can markedly re-

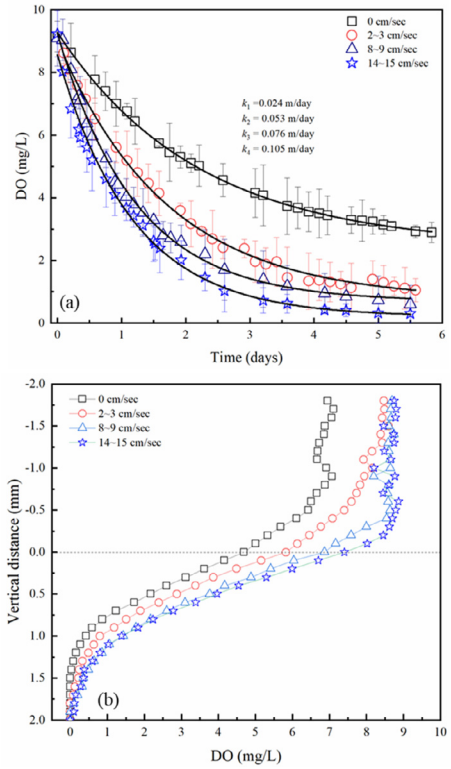

Fig. 3 – Variations in (a) dissolved oxygen (DO) concentrations and (b) O_2 profiles at the sediment-water interface (SWI) under different mixed conditions at 7 °C during SOD determination. (a) The decreased DO concentration was a first-order relationship for all mixed levels via the closed chamber values and the best fit curves were simulated using exponential regression. (b) In all the measurements, water in SOD chambers was well-oxygenated and the mm-scale distance above (–) or below (+) the SWI was selected. The SWI is indicated by the dashed line.

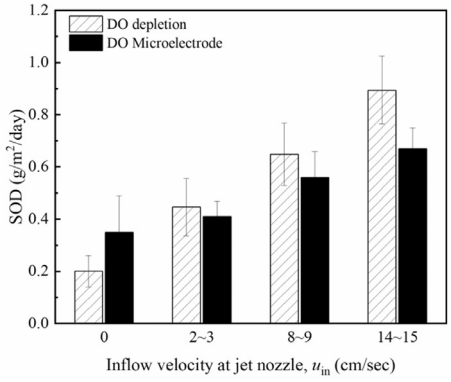

Fig. 4 – Sediment oxygen demand (SOD) values shown are the averages from the two methods (SOD_b and J_{O_2}) under different mixing conditions.

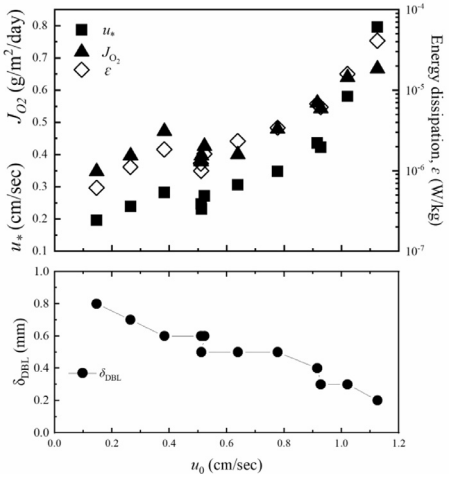

Fig. 5 – Turbulence-induced variations in currents velocity (u_0), shear velocity (u_*), energy dissipation (ε), sediment oxygen uptake (J_{O_2}), and thickness of the diffusive boundary (δ_{DBL}) values.

duce the δ_{DBL}, and extend the oxygen penetration depth into the sediment. As shown in Fig. 3b, the well-defined DBL become thinner (from 0.8 to 0.2 mm) as the inflow intensified, and the oxygen penetration depth extended from 1.3 to 2 mm.

Turbulence-induced variations in SOD values using different methods are shown in Fig. 4 to evaluate the performance and applicability of the methods for determining SOD over a range of turbulence levels. While the SOD values were increased by the u_{in} using both methods, the SOD_b values were apparently higher under mixed conditions. Under mixed conditions, the SOD_b ranged from 0.45 to 0.90 g/m^2/day and the J_{O_2} ranged from 0.35 to 0.67 g/m^2/day. The more intense the mixing, the higher SOD_b compared to J_{O_2}. However, under quiescent conditions, the average J_{O_2} was higher (0.35 g/m^2/day) than SOD_b (0.2 g/m^2/day), which may be attributed to the stirring required to obtain the average DO concentrations prior to measuring DO.

2.2. *Impact of dynamic forcing on δ_{DBL} and J_{O_2}*

Inflow-controlled variations in u_0 over the sediment enabled an assessment of the influences of turbulence on δ_{DBL} and J_{O_2}. As shown in Fig. 5, ε, u_* and J_{O_2} values increased significantly with increase in u_0 while δ_{DBL} decreased. During the experiment, the u_0 and u_* increased from 0.15 to 1.13 cm/sec and 0.196 to 0.796 cm/sec, respectively. In response to the increased turbulence levels, δ_{DBL} reduced from 0.8 mm during the weak turbulence ($\varepsilon = 6.12 \times 10^{-7}$ W/kg) to 0.2 mm during the peak turbulence ($\varepsilon = 4.1 \times 10^{-5}$ W/kg), while J_{O_2} increased from 0.35 to 0.67 g/m^2/day.

Previous studies (Arega and Lee, 2005; Bryant et al., 2011a) found that the relationship between δ_{DBL} and u_* could be expressed by Eq. (4). The δ_{DBL} data were obtained by directly observing the O_2 profiles at the SWI using microelectrode, and the corresponding u_* in response to the inflow velocity was computed using CFD models. A strong linear relationship ($r^2 = 0.863$) with a mean slope of 10.65 between δ_{DBL} and the

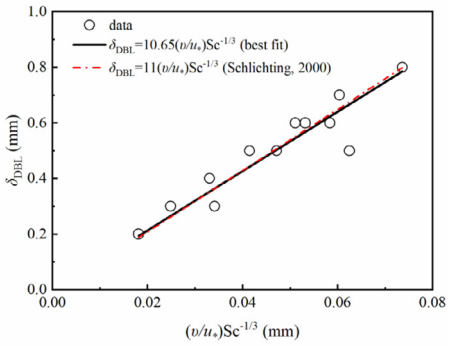

Fig. 6 – Comparison of predicted and measured boundary layer thickness.

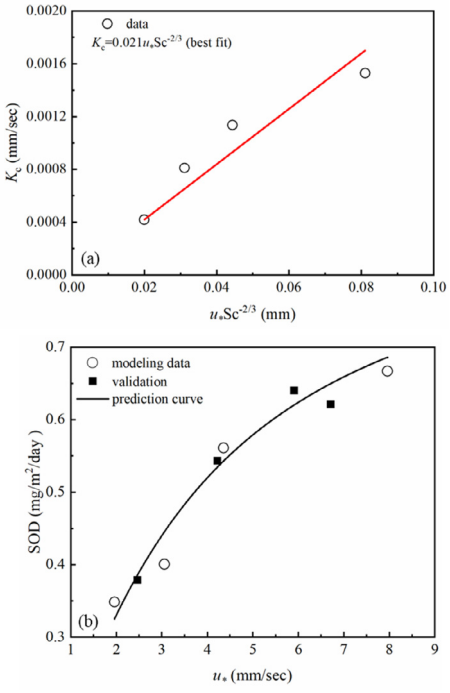

Fig. 7 – (a) Variations in the oxygen transfer coefficients in response to the turbulences at the SWI (Sc= 972.78), and (b) the comparison of predicted and measured sediment oxygen demand (SOD) as a function of the shear velocity and chamber flow rate for sediment.

viscous length function (υ/u_*) and Schmidt number (Sc) was found (Fig. 5). As currents intensified, δ_{DBL} at the water-side decreased, which can be directly observed in Fig. 3. A mean slope of 11, obtained by Bryant et al. (2011a), was consistent with our findings and indicate that δ_{DBL} at the water-side was mainly controlled by turbulence above the SWI (Fig. 6).

2.3. *Diffusional oxygen transfer and sediment oxygen demand models*

Fig. 7a shows the mean slope line of the best-fit of K_c versus $u_*Sc^{-\frac{2}{3}}$, which is 0.021 when the temperature is 7 °C and the Sc is 972.781. Based on the results and Eq. (6), the SOD then can be expressed as: $SOD = K_c\ (C_{bulk} - C_{SWI}) = f_* u_* (C_{bulk} - C_{SWI}) = 0.019 u_* (C_{bulk} - C_{SWI})$. In the above equation, the friction velocity coefficient (f_*) has a value of 0.019, which can be used as an input to the SOD model.

The SOD (using microelectrode sensors) was expressed as a function of u_* (Fig. 7b) and the constants a and b can be obtained from the best fit curves. Since C_{bulk} is stable (~8.5 mg/L), the parameter μD_s can be determined from a and f_* from b. In the present study, a and b were 0.931 and 0.406, respectively, and the corresponding μD_s and f_* were 0.051 g/m/day^2 and 0.022, respectively. Compared with the theoretical value ($f_* = 0.019$) in Section 3.5, this predict value was encouraging. Fig. 7b shows the comparison of predicted and measured SOD as a function of u_* and chamber flow rate for sediment. Modeling data were used to obtain the prediction curve to determine a and b, and more validation data were used to verify the fitness of the functions for use. As shown in Fig. 7b, the SOD prediction model is well supported by the laboratory data ($r^2 = 0.961$), and the SOD increases with velocity for all measurements.

3. Discussion

3.1. *Velocity and O_2 concentrations in overlying water*

This comprehensive study of SOD estimations in a drinking water reservoir compares two different methods for demonstrating the detailed processes of near-sediment oxygen consumption. The water current velocity vanishes at the SWI, creating a thin viscous BBL above the sediment where the currents are affected by the presence of the boundary (Tian et al., 2019). As a result, the transfer of DO through the BBL is heavily influenced by the turbulence levels and oxygen concentration in the overlaying water, especially in eutrophic and mesotrophic lakes and reservoirs with high organic matter turnover (Wüest and Lorke, 2003). Intense water currents near the sediment can result in a large increase in turbulence-induced u_* and suppression of δ_{DBL}, increasing the mass exchange (e.g., molecular diffusion, porewater convection/advection, bioturbation, and resuspension) at the SWI (Beutel, 2003; Lorke et al., 2003). Previous studies have found that velocity increases from 0 to 2–3 cm/sec over the SWI resulted in a 2- to 4-fold increase in SOD (Beutel et al., 2007; Bryant et al., 2010a). In the present study, when the u_0 increased from 0 to 1.2 cm/sec, the corresponding SOD, determined by different methods, increased 2- to 4.5-fold and J_{O_2} was smaller than that obtained from C_{bulk} by a factor of 2.

The differences between SOD determinations via different methods support the use of diffusive boundary layer models, in which not only the dissolved oxygen but also the diffusive reduced substances (e.g., dissolved iron, manganese, ammonium, and methane) are transferred across the SWI (Matzinger et al., 2010; Schwefel et al., 2018). Several studies have indicated that increased turbulences near the sediment could enhance the diffusive reduced substances flux across the sediment, further increasing the SOD (Bryant et al., 2011b; Li et al., 2019). The SOD obtained from bulk water DO concentrations in chambers acted as the total oxygen demand, while the SOD determined by J_{O_2} was merely the diffusional

oxygen transfer at the sediment. Therefore, the J_{O_2} was much smaller than what was obtained from C_{bulk} measurements as the current increased. Studies have found that the SOD was limited by the DO concentrations in the overlying water or at the SWI. The phenomenon of decreased hypolimnion oxygen demand once the overlying water DO concentration drops below 4–5 mg/L is relatively common (Beutel, 2003; Gantzer et al., 2009). The SOD models presented in this study demonstrated that the DO concentration difference between the DBL was the driving force of the diffusion which determines the diffusion flux across the SWI. The SOD was increased both within the hypolimnetic water and the sediment for almost all the oxygenation systems due to elevated hypolimnetic DO concentrations and decreased δ_{DBL} (Bierlein et al., 2017; Bryant et al., 2011a; Chen et al., 2018; Gerling et al., 2014).

3.2. *Limiting factors on SOD*

With increased u_0, the limiting SOD factor shifted from diffusion to oxygen consumption at the SWI (Beutel, 2003). Similar results were obtained by Jørgensen and Revsbech (1985); diffusional limitations on SOD were eased when turbulence was increased at the SWI (Jørgensen and Revsbech, 1985). According to the SOD models expressed by Eq. (7), the sediment oxygen consumption rate was mainly controlled by the chemical and biological components. Although some studies (Carignan and Lean, 1991; Matzinger et al., 2010) used the sediment-based reduced substances flux to estimate the hypolimnetic oxygen consumption in eutrophic lakes, the contribution of reduced substances to the SOD was relatively small (Muller et al., 2012; Steinsberger et al., 2019). Therefore, μ was considered to be the most crucial factor for SOD in sediment; the SOD increases with μ. Nevertheless, the dependence of SOD on oxygen consumption in the sediment was not as strong as the dependence on fluid flow (Higashino, 2011). Moreover, when the μ was small, increased current over the sediment had a negligible impact on the SOD, and SOD approached a constant value rapidly as u_* increased (Higashino, 2018). The biological oxygen consumption in sediment was also constrained by the amount and quality of organic matters (Steinsberger et al., 2017). In most cases, the μ is typically high in the shallower regions of reservoirs and lakes where organic matter is easily degradable, and the DO concentrations remain high. Conversely, the μ decreases in deeper sediments with more factory organic carbon and lower DO concentrations (Schwefel et al., 2018).

In the present study, the sediment was collected in the main basin of a canyon-shaped drinking water reservoir having very steep slopes, such that the hypolimnion depths were approximately the same. According to Section 2.3, the parameter μD_s was 0.051 g/m/day^2 and μ was 418.3 g/m^3/day when $D_s = 1.41 \times 10^{-9}$ m^2/sec at 7 °C. The linear dependence of SOD on u_* for low velocity conditions has been confirmed in well-oxygenated overlying waters by previous studies (Higashino, 2018; Mackenthun and Stefan, 1998). This was confirmed by the present study as well (Fig. 5). When u_* increased markedly, SOD approached a constant value (SOD = $\sqrt{2\mu D_s C_{bulk}}$), which is a function μ and independent of u_* (Higashino, 2018). According to this simplified estimation, the increase in SOD under well-oxygenated and strong turbulent conditions (e.g., hypolimnetic oxygenation and artificial destratification) can be obtained as SOD = 0.985 mg/m^2/day. The modelling results are practical and can aid when designing hypolimnetic aeration systems and managing the water quality in reservoirs.

4. Conclusions

A model of SOD for a deep canyon-shaped reservoir was developed. The results of different methods revealed the effect of hydraulics on diffusive boundary layers and the corresponding SOD at the SWI. The dependence of the oxygen transfer coefficient (K_c) and the diffusive boundary layer thickness (δ_{DBL}) on the hydraulic parameters (e.g., υ, u_*, and Sc) were quantified, and the SOD was expressed as a function of the shear velocity (u_*) and the bulk DO concentration (C_{bulk}). Theoretical predictions were validated by microelectrode measurements in a series of laboratory experiments.

The present study focused on building an integrated SOD models by comparing the DO depletion in a closed chamber (SOD_b) and sediment oxygen uptake (J_{O_2}) at the SWI. Our results revealed that increased benthic currents could enhance the fluxes of diffusive reduced substances, further increasing the SOD at the SWI. When the maximum biological oxygen consumption rate was constant (μ = 418.3 g/m^3/day at 7 °C), an increased current over the sediment raised the SOD 4.5-fold compared to that over stagnant water. The critical control that near-sediment current velocity has on SOD must be considered when designing and implementing aeration/artificial mixing management strategies.

Acknowledgements

This work was supported by the Natural Science Foundation of China (No. 51979217).

REFERENCES

Arega, F., Lee, J.H.W., 2005. Diffusional mass transfer at sediment–water interface of cylindrical sediment oxygen demand chamber. J. Environ. Eng. 131 (5), 755–766. doi:10.1061/(asce)0733-9372(2005)131:5(755).

Beutel, M., Dent, S., Reed, B., Marshall, P., Gebremariam, S., Moore, B., et al., 2014. Effects of hypolimnetic oxygen addition on mercury bioaccumulation in Twin Lakes, Washington, USA. Sci. Total Environ. 496, 688–700. doi:10.1016/j.scitotenv.2014.06.117.

Beutel, M., Hannoun, I., Pasek, J., Bowman Kavanagh, K., 2007. Evaluation of hypolimnetic oxygen demand in a large eutrophic raw water reservoir, san vicente reservoir. Calif. J. Environ. Eng. 133 (2), 130–138. doi:10.1061/(ASCE)0733-9372(2007)133:2(130).

Beutel, M.W., 2003. Hypolimnetic anoxia and sediment oxygen demand in california drinking water reservoirs. Lake Reserv. Manag. 19 (3), 208–221. doi:10.1080/07438140309354086.

Bierlein, K.A., Rezvani, M., Socolofsky, S.A., Bryant, L.D., Wüest, A., Little, J.C., 2017. Increased sediment oxygen flux in lakes and reservoirs: the impact of hypolimnetic oxygenation. Water Resour. Res. 53 (6), 4876–4890. doi:10.1002/2016WR019850.

Bouldin, D.R., 1968. Models for describing the diffusion of oxygen and other mobile constituents across the mud-water interface. J. Ecol. 56 (1), 77. doi:10.2307/2258068.

Bowman, G., Delfino, J., 1980. Sediment oxygen demand techniques: a review and comparison of laboratory and in situ systems. Water Res. 14, 491–499. doi:10.1016/0043-1354(80)90215-8.

Bryant, L.D., Gantzer, P.A., Little, J.C., 2011a. Increased sediment oxygen uptake caused by oxygenation-induced hypolimnetic mixing. Water Res. 45 (12), 3692–3703. doi:10.1016/j.watres.2011.04.018.

Bryant, L.D., Hsu-Kim, H., Gantzer, P.A., Little, J.C., 2011b. Solving the problem at the source: controlling Mn release at the sediment-water interface via hypolimnetic oxygenation. Water Res. 45 (19), 6381–6392. doi:10.1016/j.watres.2011.09.030.

Bryant, L.D., Lorrai, C., McGinnis, D.F., Brand, A., Wüest, A., Little, J.C., 2010a. Variable sediment oxygen uptake in response to dynamic forcing. Limnol. Oceanogr. 55 (2), 950–964. doi:10.4319/lo.2009.55.2.0950.

Bryant, L.D., McGinnis, D.F., Lorrai, C., Brand, A., Little, J.C., Wüest, A., 2010b. Evaluating oxygen fluxes using microprofiles from both sides of the sediment-water interface. Limnol. Oceanogr. Meth. 8 (11), 610–627. doi:10.4319/lom.2010.8.0610.

Carignan, R., Lean, D.R.S., 1991. Regeneration of dissolved substances in a seasonally anoxic lake: the relative importance of processes occurring in the water column and in the sediments. Limnol. Oceanogr. 36, 683–707. doi:10.2307/2837566.

Chen, S., Little, J.C., Carey, C.C., McClure, R.P., Lofton, M.E., Lei, C., 2018. Three-dimensional effects of artificial mixing in a shallow drinking-water reservoir. Water Resour. Res. 54 (1), 425–441. doi:10.1002/2017WR021127.

Dutton, C.L., Subalusky, A.L., Hamilton, S.K., Rosi, E.J., Post, D.M., 2018. Organic matter loading by hippopotami causes subsidy overload resulting in downstream hypoxia and fish kills. Nat. Commun. 9 (1), 1951. doi:10.1038/s41467-018-04391-6.

Gantzer, P.A., Bryant, L.D., Little, J.C., 2009. Effect of hypolimnetic oxygenation on oxygen depletion rates in two water-supply reservoirs. Water Res. 43 (6), 1700–1710. doi:10.1007/s10750-009-9705-0.

Gerling, A.B., Browne, R.G., Gantzer, P.A., Mobley, M.H., Little, J.C., Carey, C.C., 2014. First report of the successful operation of a side stream supersaturation hypolimnetic oxygenation system in a eutrophic, shallow reservoir. Water Res. 67, 129–143. doi:10.1016/j.watres.2014.09.002.

Zhang, Haihan, Zong, Rongrong, He, Huiyan, Liu, Kaiwen, Yan, Miaomiao, Miao, Yutian, et al., 2021. Biogeographic distribution pattern of algal community structure in different urban lakes of China: insights into dynamics and co-existence. J. Environ. Sci. 100, 216–227. doi:10.1016/j.jes.2020.07.024.

Higashino, M., 2018. Oxygen transfer at the sediment/water interface for sediment bed with rough surface. J. Geophys. Res. Biogeogr. 123, 3283–3292. doi:10.1029/2018JG004602.

Higashino, M., O'Connor, B., Hondzo, M., Stefan, H., 2008. Oxygen transfer from flowing water to microbes in an organic sediment bed. Hydrobiologia 614 (1), 219–231. doi:10.1007/s10750-008-9508-8.

Higashino, M.J.W.R., 2011. Oxygen consumption by a sediment bed for stagnant water: comparison to SOD with fluid flow. Water Res. 45 (15), 4381–4389. doi:10.1016/j.watres.2011.04.051.

Ito, Y., Momii, K., 2015. Impacts of regional warming on long-term hypolimnetic anoxia and dissolved oxygen concentration in a deep lake. Hydrol. Process. 29, 2232–2242. doi:10.1002/hyp.10362.

Jabbari, A., Boegman, L., Valipour, R., Wain, D., Bouffard, D., 2020. Dissipation of turbulent kinetic energy in the oscillating bottom boundary layer of a large shallow lake. J. Atmos. Ocean. Technol. 37. doi:10.1175/JTECH-D-19-0083.1.

Jørgensen, B., Revsbech, N., 1985. Diffusive boundary layers and the oxygen uptake of sediments and detritus. Limnol. Oceanogr. 30 (1), 111–122. doi:10.4319/lo.1985.30.1.0111.

Li, N., Huang, T., Mao, X., Zhang, H., Li, K., Wen, G., et al., 2019. Controlling reduced iron and manganese in a drinking water reservoir by hypolimnetic aeration and artificial destratification. Sci. Total Environ. 685, 497–507. doi:10.1016/j.scitotenv.2019.05.445.

Lorke, A., Müller, B., Maerki, M., Wüest, A., 2003. Breathing sediments: The control of diffusive transport across the sediment—water interface by periodic boundary-layer turbulence. Limnol. Oceanogr. 48, 2077–2085. doi:10.2307/3597808.

Mackenthun, A.A., Stefan, H.G., 1998. Effect of flow velocity on sediment oxygen demand. J. Environ. Eng. 124 (3), 222–230. doi:10.1061/(ASCE)0733-9372(1998)124:3(222).

Matzinger, A., Müller, B., Niederhauser, P., Schmid, M., Wüest, A., 2010. Hypolimnetic oxygen consumption by sediment-based reduced substances in former eutrophic lakes. Limnol. Oceanogr. 55 (5), 2073–2084. doi:10.4319/lo.2010.55.5.2073.

Muller, B., Bryant, L.D., Matzinger, A., Wuest, A., 2012. Hypolimnetic oxygen depletion in eutrophic lakes. Environ Sci Technol 46 (18), 9964–9971. doi:10.1021/es301422r.

Schwefel, R., Hondzo, M., Wüest, A., Bouffard, D., 2017. Scaling oxygen microprofiles at the sediment interface of deep stratified waters. Geophys. Res. Lett. 44 (3), 1340–1349. doi:10.1002/2016GL072079.

Schwefel, R., Steinsberger, T., Bouffard, D., Bryant, L.D., Müller, B., Wüest, A., 2018. Using small-scale measurements to estimate hypolimnetic oxygen depletion in a deep lake. Limnol. Oceanogr. 63 (S1), S54–S67. doi:10.1002/lno.10723.

Steinsberger, T., Müller, B., Gerber, C., Shafei, B., Schmid, M., 2019. Modeling sediment oxygen demand in a highly productive lake under various trophic scenarios. PLoS ONE 14 (10), e0222318. doi:10.1371/journal.pone.0222318.

Steinsberger, T., Schmid, M., Wuest, A., Schwefel, R., Wehrli, B., Müller, B., 2017. Organic carbon mass accumulation rate regulates the flux of reduced substances from the sediments of deep lakes. Biogeosciences 14, 3275–3285. doi:10.5194/bg-14-3275-2017.

Tian, H., Li, Q., Pan, M., Zhou, Q., Dong, Y., 2019. High-Schmidt-number dissolved oxygen transfer from turbulent flows to permeable microbial sediment bed. Adv. Water Resour. 125, 1–12. doi:10.1016/j.advwatres.2019.01.005.

Wüest, A., Lorke, A., 2003. Small-Scalehydrodynamics In lakes. Annu. Rev. Fluid Mech. 35 (1), 373–412. doi:10.1146/annurev.fluid.35.101101.161220.

Wüest, A., Piepke, G., Van Senden, D.C., 2000. Turbulent kinetic energy balance as a tool for estimating vertical diffusivity in wind-forced stratified waters. Limnol. Oceanogr. 45, 1388–1400. doi:10.2307/2670531.

Yan, M.M., Chen, S.N., Huang, T.L., Li, B.Q., Li, N., Liu, K.W., et al., 2020. Community compositions of phytoplankton and eukaryotes during the mixing periods of a drinking water reservoir: dynamics and interactions. Int. J. Environ. Res. Public Health 17, 1128. doi:10.3390/ijerph17041128.